

COMPUTATIONAL FLUID DYNAMICS OF UNSTEADY AERODYNAMIC
WAKE ON HELICOPTER MAIN ROTOR-HUB ASSEMBLY

NURAIN BINTI OTHMAN

A thesis submitted in fulfilment of the
requirements for the award of the degree of
Master of Philosophy

School of Mechanical Engineering
Faculty of Engineering
Universiti Teknologi Malaysia

FEBRUARY 2022

DEDICATION

I dedicated this thesis to my father, Othman Bakar who taught me knowledge best learnt the hard way and my mother, Saitom Idris who taught me that the hardest tasks can be accomplished if you just take one step at a time. My siblings Hamka, Afifi, and Haqim that always supported me even in my craziest time and not forgetting my friends Mukah, Aiman and Gaspar who always offered me his best thoughts on opinions on my work.

ACKNOWLEDGEMENT

In preparing this thesis, I was contacted and helped by researchers, academicians, and friends. They contributed ideas and knowledge towards my works. I wish to express my sincere gratitude to my main supervisor, Dr. Iskandar Shah Ishak for his encouragements, critics and guidance in completing these works. I am also thankful to my co-supervisor Dr Nizam Dahalan for his patient, guidance, advices and motivations. Without their supports, this thesis will not come to light.

I would like to thank Dr Wan Zaidi Wan Omar, for his supports and my parents, Encik Othman Bakar and Puan Saitom Idris for always inspires me to work harder and keep moving forward one at a time. I am also blessed to all my family members who always keep me motivate in finishing what I started.

My fellow postgraduate students that had provided their assistances at various occasions and useful tips. Thank you.

ABSTRACT

Flow field on the helicopter is intricate and has puzzled aerodynamicists for decades. Tail shake problem has become an issue since the creation of helicopters, where it has caused tremors on the structure of the helicopter, performance, occupant's comfort and interrupted the control, response and quality of the flight. It has been the continuous issues for designers and researchers in improving flight quality and better helicopter performance. However, previous researches focused on unsteady helicopter rotor hub wake at low range advance ratios merely up to 0.3 where the air load pressure was believed to be too small to influence the flow surrounding at the vicinity of tail parts. Therefore, simulation work beyond 0.3 is much required to investigate the unsteady flow characteristics at higher advance ratios. The aim of this research was to identify the aerodynamic characteristics elicited by the unsteady wake of the helicopter's main rotor hub-assembly at higher advanced ratios beyond 0.3 through observations on static and dynamic analyses. The parameters investigated were the rotational speeds of 1200, 1400 and 1600 rpm, with two, three and four main rotor blades, two different fairing configurations and four different angles of attack (α). Rotor aerodynamics was modelled using Computational Fluid Dynamics by employing sliding mesh method to account for rotor rotation and $k-w$ Shear Stress Transport for turbulent modelling. The results were collected in percentage and compared with calculation that had been done through experimental works by other researchers. The data collected were pressure fluctuation, turbulent kinetic energy, turbulent intensity and drag force. Dynamic analysis focused on the power spectral density, which showed the wake amplitude formation in the frequency domain. In general, turbulent kinetic energy for four blades rotor components showed higher values as compared to two blades, three blades and fuselage components. Turbulent kinetic energy recorded maximum value from $3.0 \text{ m}^2/\text{s}^2$ to $4.0 \text{ m}^2/\text{s}^2$ fuselage and $6.4 \text{ m}^2/\text{s}^2$ to $10 \text{ m}^2/\text{s}^2$ for rotor for elliptical fairing and $6.8 \text{ m}^2/\text{s}^2$ to $13 \text{ m}^2/\text{s}^2$ and $14 \text{ m}^2/\text{s}^2$ to $22 \text{ m}^2/\text{s}^2$ for rectangular fairing. Turbulent kinetic energy and turbulent intensity were effected by the number of blades, rotational speed, angle of attack and geometry of fairings. Drag force sourced out from the fuselage created 29% to 70% while the rotor produce 30% to 45% of drag. For dynamic analysis, turbulent kinetic energy of rectangular fairing showed a high wake amplitude of $7268.5 \text{ (m}^4/\text{s}^4)/\text{Hz}$, while turbulent kinetic energy of elliptical fairing showed wake amplitude of $7285.3 \text{ (m}^4/\text{s}^4)/\text{Hz}$, which showed the effect of complex geometry on the turbulent formation. Furthermore, the simulation conducted on the actual rotor hub indicated that a rotational speed of 1200 rpm has the highest value of turbulent kinetic energy of $42.7 \text{ (m}^4/\text{s}^4)/\text{Hz}$ without the fairing employment. Employment of fairing has proven to reduce the formation of wake frequency. The results from 1200 rpm rotational speed were successfully validated with past researchers' results in predicting the wake formation based on the frequency domain. In conclusion, the study successfully showed that the formation of unsteady wake sourced from a simplified model helicopter drawn and proved the presence of fairing does reduce the wake formation on the aft of the fuselage. Subsequently, this research proposes that three rotor blades with an elliptical fairing configuration is the best configuration with the lowest wake formation.

ABSTRAK

Medan aliran pada helikopter adalah rumit dan telah membingungkan ahli aerodinamik sekian lama. Masalah getaran pada ekor helikopter telah menjadi isu sejak penciptaannya, yang mana ia telah menyebabkan gegaran pada struktur helikopter, pengurangan prestasi, keselesaan penumpang, mengganggu kawalan, tindak balas dan kualiti penerbangan. Ia telah menjadi isu berterusan dalam menambah baik ke arah penerbangan berkualiti dan helicopter berprestasi lebih baik. Walaubagaimanapun, fokus kajian terdahulu mengenai pemutar had keracak helikopter yang tidak stabil telah dilakukan pada julat rendah nisbah mara sehingga 0.3 yang mana beban tekanan udara dipercayai terlalu kecil untuk helikopter mempengaruhi aliran sekeliling di sekitar bahagian ekor. Oleh itu, kerja simulasi melebihi 0.3 amat diperlukan untuk menyelidiki ciri aliran tidak mantap pada nisbah mara yang lebih tinggi. Tujuan penyelidikan ini adalah untuk mengenal pasti ciri-ciri aerodinamik yang terkesan disebabkan keracak tidak-tetap dari pemasangan hab pemutar utama helikopter pada nisbah lebih tinggi melebihi 0.3 melalui pemerhatian pada analisis statik dan dinamik. Parameter yang disiasat adalah kelajuan pada putaran 1200, 1400 dan 1600 rpm, dengan dua, tiga dan empat bilangan bilah pemutar utama, dua konfigurasi reraut berbeza dan empat sudut serang (α) yang berbeza. Pemutar aerodinamik dimodelkan menggunakan kaedah jejaring gelangar untuk putaran hab pemutar dan pemodelan gelora *k-w Shear Stress Transport*. Keputusan dikumpul melalui kadar peratus dan telah dibandingkan dengan pengiraan yang dilakukan melalui kerja-kerja eksperimen oleh penyelidik lain. Bentuk data yang dikumpul adalah perubahan tekanan, gelora tenaga kinetik, keampatan gelora dan daya seretan. Analisis dinamik memberi tumpuan kepada ketumpatan spektrum kuasa, yang menunjukkan pembentukan amplitud terhadap domain frekuensi. Secara umumnya, gelora tenaga kinetik bagi komponen dengan empat bilah menunjukkan nilai yang lebih tinggi berbanding dengan dua, tiga bilah dan komponen fuslaj. Gelora tenaga kinetik mencatatkan nilai maksimum dari $3.0 \text{ m}^2/\text{s}^2$ hingga $4.0 \text{ m}^2/\text{s}^2$ untuk fuslaj dan $6.4 \text{ m}^2/\text{s}^2$ hingga $10 \text{ m}^2/\text{s}^2$ untuk pemutar bagi reraut elips dan $6.8 \text{ m}^2/\text{s}^2$ hingga $13 \text{ m}^2/\text{s}^2$ dan $14 \text{ m}^2/\text{s}^2$ hingga $22 \text{ m}^2/\text{s}^2$ untuk reraut segi empat tepat. Gelora tenaga kinetik dan keampatan gelora terbukti dipengaruhi oleh bilangan bilah, kelajuan putaran bilah, sudut serang dan geometri reraut. Daya seret yang diperoleh daripada fuslaj memenuhi keputusan data yang dikumpul oleh penyelidik lain bahawa ia menghasilkan 29% hingga 70% daya seretan manakala pemutar menghasilkan 30% hingga 45%. Manakala, analisis dinamik reraut segi empat tepat untuk gelora tenaga kinetik menunjukkan amplitud yang tinggi sebanyak $7268.5 ((\text{m}^4/\text{s}^4)/\text{Hz})$, bahkan reraut elips untuk gelora tenaga kinetik menunjukkan amplitud setinggi $7285.3 ((\text{m}^4/\text{s}^4)/\text{Hz})$, menunjukkan kesan geometri yang rumit membantu dalam penghasilan dan pembentukan gelora. Tambahan pula, simulasi yang dilakukan pada hab bilah sebenar menunjukkan bahawa 1200 rpm mempunyai nilai gelora tenaga kinetik tertinggi iaitu $42.7 ((\text{m}^4/\text{s}^4)/\text{Hz})$ tanpa pemasangan reraut. Penggunaan reraut terbukti dapat mengurangkan pembentukan kekerapan gelora. Hasil daripada kelajuan putaran 1200 rpm telah berjaya disahkan dengan penyelidik lepas dalam pengiraan pembentukan amplitud berdasarkan domain frekuensi. Kesimpulannya, kajian telah membuktikan kehadiran reraut dapat mengurangkan pembentukan keracak tidak-tetap pada fuslaj dan mencadangkan tiga bilah pemutar reraut elips adalah model konfigurasi helikopter terbaik dengan kadar pembentukan dan penghasilan gelora terendah.

TABLE OF CONTENTS

TITLE	PAGE
DECLARATION	iii
DEDICATION	iv
ACKNOWLEDGEMENT	v
ABSTRACT	vi
ABSTRAK	vii
TABLE OF CONTENTS	vii
LIST OF TABLES	x
LIST OF FIGURES	xiv
CHAPTER 1 INTRODUCTION	1
1.1 Background	1
1.2 Importance of Rotor System	2
1.3 Interaction of Unsteady Wake	3
1.4 Problem statement	8
1.5 Objectives	9
1.6 Scopes of Study	10
CHAPTER 2 LITERATURE REVIEW	11
2.1 Introduction	11
2.2 Flight Configurations	19
2.3 Rotor Advance Ratio, μ	20
CHAPTER 3 METHOD OLOGY	25
3.1 Introduction	25
3.1.2 Blade-stubs Configurations	26
3.1.3 Fuselage Geometry	29
3.1.4 Number of Blades Configurations	30
3.1.5 Fairing configurations	33
3.2 Numerical Approach	35

3.2.1	Introduction	35
3.2.2	Preliminary Works on Airfoil	36
3.2.3	Pre-process setup for NACA 0012	36
3.2.3.1	Geometry	36
3.2.4	Grid Independent Study (GIS)	37
3.2.5	Turbulence modelling	38
3.2.6	Validation of the simulation	40
CHAPTER 4 RESULTS AND DISCUSSIONS		47
4.1	Overview	47
4.2	Reference LoCations of Measurement	47
4.3	Contour Plot	49
4.4	Static Analysis	50
4.4.1	Elliptical Fairing	50
4.4.1.1	Two Blades Rotor Hub Assembly	50
4.4.1.2	Three Blades Rotor Hub Assembly	62
4.4.1.3	Four Blades Rotor Hub Assembly	71
4.4.1.4	Summary	79
4.4.2	Rectangular Fairing	84
4.4.2.1	Static Analysis	84
4.4.2.2	Dynamic pressure	84
4.4.2.3	Total pressure	90
4.4.2.4	Turbulent kinetic energy	93
4.4.2.5	Turbulent intensity	98
4.4.2.6	Drag force	101
4.4.2.7	Summary	102
4.4.2.8	Comparison elliptical and rectangular static analysis	104
4.4.3	Real Rotor Hub Assembly	108
4.4.3.1	Dynamic pressure	109
4.4.3.2	Total pressure	111
4.4.3.3	Turbulent kinetic energy	114
4.4.3.4	Turbulent intensity	115

4.4.3.5	Drag force	117
4.4.3.6	Summary	118
4.5	Dynamic Analysis	120
4.5.1	Elliptical Fairing	120
4.5.2	Turbulent kinetic energy	121
4.5.2.1	Power spectral density turbulent kinetic energy	126
4.5.2.2	Turbulent intensity	128
4.5.2.3	Summary	132
4.5.3	Rectangular Fairing	135
4.5.3.1	Turbulent kinetic energy	135
4.5.3.2	Turbulent intensity	138
4.5.3.3	Summary	142
4.5.4	Actual Rotor Hub Assembly	145
4.5.4.1	Rotational Speed 1600 rpm	145
4.5.4.2	Rotational Speed 1400 rpm	149
4.5.4.3	Rotational Speed 1200 rpm	153
4.6	No Fairing Simplified Model	159
4.6.1	Summary	160
CHAPTER 5 CONCLUSIONS AND RECOMMEN DATIONS		165
5.1.	Static Analysis	165
5.1.	Dynamic Analysis	166
5.3	Research Contribution	167
5.4	Recommendation for Future Work	168
REFERENCES		169
LIST OF PUBLICATIONS		175

LIST OF TABLES

TABLE NO.	TITLE	PAGE
Table 2.1	Helicopter advance ratio selected parameters.	22
Table 3.1	Parameters set up on Ansys	40
Table 4.1	Facet maximum dynamic pressure 2 blades static analysis.	51
Table 4.2	Facet maximum total pressure 2 blades static analysis.	52
Table 4.3	Facet maximum turbulent kinetic energy 2 blades static analysis	55
Table 4.4	Facet maximum turbulent intensity 2 blades static analysis.	56
Table 4.5	Facet maximum turbulent dissipation rate ϵ 2 blades static analysis.	56
Table 4.6	Dynamic and total pressure at -5 and -20 degree angles for 2 blades angle of attack.	58
Table 4.7	Turbulent kinetic energy, and intensity at -5 and -20 degree for 2 blade static analysis.	61
Table 4.8	Drag force at -5 and -20 degree angles of attack for 2 blades static analysis	62
Table 4.9	Facet maximum dynamic pressure 3 blades static analysis	64
Table 4.10	Facet maximum total pressure 3 blades static analysis	65
Table 4.11	Dynamic and total pressure at -5 and -20 degree angles of attack for 3 blades elliptical static analysis	66
Table 4.12	Facet maximum turbulent kinetic energy 3 blades static analysis	67
Table 4.13	Facet maximum turbulent intensity 3 blades static analysis	69
Table 4.14	Turbulent kinetic energy and turbulent intensity at -5 and -20 degree angles of attack for 3 blades static analysis	70
Table 4.15	Drag force of 3 blades rotor hub assembly for static analysis	70
Table 4.16	Facet maximum dynamic pressure for 4 blades static analysis	72
Table 4.17	Dynamic pressure and total pressure of -5 and -20 degree angles of attack for 4 blades static analysis.	73
Table 4.18	Facet maximum total pressure for 4 blades static analysis	74

Table 4.19	Facet maximum turbulent kinetic energy for 4 blades static analysis.	76
Table 4.20	Facet maximum turbulent intensity for 4 blades static analysis	77
Table 4.21	Turbulent kinetic energy and turbulent intensity of -5 and -20 angles of attack for 4 blades static analysis	78
Table 4.22	Drag force for elliptical fairing 4 blades rotor assembly static analysis	78
Table 4.23	Facet maximum dynamic pressure 2 blades rectangular fairing static analysis.	87
Table 4.24	Facet maximum dynamic pressure 3 blades rectangular fairing static analysis.	87
Table 4.25	Facet maximum dynamic pressure 4 blades rectangular fairing static analysis	88
Table 4.26	Dynamic pressure and total pressure of -5 and -20 degree angles of attack for rectangular fairing 2 blades static analysis	88
Table 4.27	Dynamic pressure and total pressure of -5 and -20 angles of attack for rectangular fairing 3 blades static analysis	89
Table 4.28	Dynamic pressure and total pressure of -5 and -20 degree angles of attack for rectangular fairing 4 blades static analysis.	89
Table 4.29	Facet maximum total pressure 2 blades rectangular fairing static analysis	92
Table 4.30	Facet maximum total pressure 3 blades rectangular fairing static analysis	92
Table 4.31	Facet maximum total pressure 4 blades rectangular fairing static analysis	93
Table 4.32	Facet maximum turbulent kinetic energy 2 blades rectangular fairing static analysis	95
Table 4.33	Facet maximum turbulent kinetic energy 3 blades rectangular fairing static analysis	96
Table 4.34	Facet maximum turbulent kinetic energy 4 blades rectangular fairing static analysis	96
Table 4.35	Turbulent kinetic energy and turbulent intensity of -5 and -20 angles of attack for rectangular fairing 2 blades static analysis	97
table 4.36	Turbulent kinetic energy and turbulent intensity of -5 and -20 angles of attack for rectangular fairing 3 blades static	

	analysis	97
Table 4.37	Turbulent kinetic energy and turbulent intensity of -5 and -20 degree angles of attack for rectangular fairing 4 blades static analysis	98
Table 4.38	Facet maximum turbulent intensity 2 blades rectangular fairing static analysis	100
Table 4.39	Facet maximum turbulent intensity 3 blades rectangular fairing static analysis	100
Table 4.40	Facet maximum turbulent intensity 4 blades rectangular fairing static analysis	101
Table 4.41	Drag force for rectangular fairing 2 blades rotor assembly static analysis	101
Table 4.42	Drag force for rectangular fairing 3 blades rotor assembly static analysis	102
Table 4.43	Drag force for rectangular fairing 4 blades rotor assembly static analysis	102
Table 4.44	Facet maximum dynamic pressure real rotor static analysis	111
Table 4.45	Facet maximum total pressure real rotor static analysis	112
Table 4.46	Dynamic pressure and total pressure for real rotor static analysis	113
Table 4.47	Facet maximum turbulent kinetic energy real rotor static analysis	115
Table 4.48	Facet maximum turbulent intensity actual rotor static analysis	116
Table 4.49	Turbulent kinetic energy and turbulent intensity actual rotor static analysis	117
Table 4.50	Drag force actual rotor static analysis	117
Table 4.51	RMS facet maximum turbulent kinetic energy elliptical fairing dynamic analysis	125
Table 4.52	RMS facet maximum turbulent intensity elliptical fairing dynamic analysis	130
Table 4.53	RMS facet maximum turbulent kinetic energy rectangular fairing dynamic analysis	137
Table 4.54	RMS facet maximum turbulent intensity rectangular fairing dynamic analysis	140
Table 4.55	RMS facet maximum turbulent kinetic energy for 1600 rpm rotational speed.	147
Table 4.56	PSD turbulent kinetic energy for 1600 rpm.	148

Table 4.57	RMS turbulent intensity for 1600 rpm.	148
Table 4.58	Wake turbulent intensity for 1600 rpm	149
Table 4.59	RMS turbulent kinetic energy 1400 rpm	150
Table 4.60	Wake turbulent kinetic energy for 1400 rpm	151
Table 4.61	RMS turbulent intensity 1400 rpm	152
Table 4.62	Wake turbulent intensity for 1400 rpm	153
Table 4.63	RMS facet maximum dynamic pressure 1200 rpm	154
Table 4.64	RMS facet maximum total pressure 1200 rpm	155
Table 4.65	RMS turbulent kinetic energy for 1200 rpm	157
Table 4.66	RMS turbulent intensity for 1200 rpm	158

LIST OF FIGURES

FIGURE NO.	TITLE	PAGE
Figure 1	Anti-torque rotor produces thrust to oppose torque (FAA, 2012).	3
Figure 1.1	Main rotor hub assembly (FAA, 2012).	4
Figure 1.2	Velocity differences along the main rotor blades	5
Figure 1.3	Velocity difference between the tip and the centre of the rotation.	6
Figure 1.4	Schematic of tail shake phenomenon (Waard and Trouvé, 1999)	7
Figure 2.1	Schematic diagram of rotor hub wake's trajectories (Ishak, 2012)	12
Figure 2.2	Turbulent formation during yawing orientation	13
Figure 2.3	Blade-stubs configuration (Ishak, 2012)	14
Figure 2.4	Power Density Function analysis on different pylon configuration at advance ratio 0.35 and 1400 rpm (Ishak, 2012).	15
Figure 2.5	Experimental set-up (Ishak, 2012).	15
Figure 2.6	Full equipped model (De Gregorio and Cinquegrana, 2010)	16
Figure 2.7	Rotor and empennage modeled with wake-shedding lifting surfaces (Rex W. <i>et. al.</i> , 2020).	17
Figure 2.8	Comparison of baseline fuselage geometry (left) and modified fuselage (right) showing the blending of engine cowl with shaft fairings. (Khier, 2012)	18
Figure 2.9	Left: Hub fairing shapes. Right: Hub fairing cross sections. (Khier 2012)	18
Figure 2.10	Helicopter at yawed (Ishak <i>et. al.</i> , 2012)	20
Figure 2.11	Propeller efficiency performance at different advance ratio (Yu, 2017)	21
Figure 3.1	Blade-stubs configurations (Khier, 2012).	26
Figure 3.2	Four blades stubs configurations for simplified model.	27
Figure 3.3	Blade stubs configuration done by Stepanov <i>et. al.</i> (2016).	27
Figure 3.4	Blade stubs configuration done by Raghav <i>et. al.</i> (2013)	28

Figure 3.5	An ellipsoidal fuselage.	29
Figure 3.6	Two blade-stubs	30
Figure 3.7	Three blade-stubs	31
Figure 3.8	Dimension of simplified main-rotor-hub (side view).	31
Figure 3.9	Dimension for simplified main-rotor-hub.	31
Figure 3.10	Real dimension structure.	32
Figure 3.11	Close-up view of the real rotor structure.	32
Figure 3.12	Standard simplified fuselage attached with blade-stubs (Ishak, 2012).	33
Figure 3.13	Isometry view of real dimension.	33
Figure 3.14	Rectangular pylon with simplified main-rotor-hub.	34
Figure 3.15	Elliptical pylon configuration with simplified main rotor-hub assembly.	35
Figure 3.16	NACA 0012 with the dimension of a 1-meter chord and 1-meter wingspan.	37
Figure 3.17	Computational domain around NACA 0012 (Ahmed, 2013).	37
Figure 3.18	Grid independent study at $\alpha = -15^\circ$.	38
Figure 3.19	Variation of Pressure coefficient for $\alpha = -10^\circ$ for $Re = 3 \times 10^6$	39
Figure 3.20	Variation of Pressure coefficient for NACA 0012 at $\alpha = 0^\circ$ for $Re = 3 \times 10^6$.	40
Figure 3.21	Variation of Pressure coefficient for NACA 0012 $\alpha = 0^\circ$ for $Re = 9 \times 10^6$.	41
Figure 3.22	Variation of Pressure coefficient for NACA 0012 at $\alpha = 0^\circ$ for $Re = 6 \times 10^6$.	41
Figure 3.23	Flowchart of research methodology	42
Figure 3.24	Physical domain.	44
Figure 3.25	Computational domain.	45
Figure 4.1	Side plane reference	48
Figure 4.2	Top plane reference	48
Figure 4.3	Side plane area of analysis	49
Figure 4.4	Top plane area of analysis	49
Figure 4.5	Contour plot dynamic pressure 2 blades rotor assemblies x	50

Figure 4.6	Pressure drop zone shown (positive values blanked) (Khier, 2012)	51
Figure 4.7	Contour plot total pressure 2 blades rotor assemblies	52
Figure 4.8	Contour plot turbulent kinetic energy 2 blades rotor assemblies	54
Figure 4.9	Contour plot turbulent intensity 2 blades rotor assemblies	54
Figure 4.10	Dynamic pressure of fuselage and rotor components	57
Figure 4.11	Point 1 and 2 of fuselage	57
Figure 4.12	Point 3 of rotor assembly	57
Figure 4.13	Total pressure of fuselage and rotor components	59
Figure 4.14	Turbulent kinetic energy for fuselage components	60
Figure 4.15	Turbulent intensity for fuselage components	60
Figure 4.16	Side plane of 3 blades simplified model.	63
Figure 4.17	Contour plot dynamic pressure 3 blades rotor hub assembly	63
Figure 4.18	Dynamic pressure for fuselage components	64
Figure 4.19	Contour plot total pressure 3 blades rotor hub assembly	65
Figure 4.20	Total pressure for fuselage component for 3 blades static analysis.	66
Figure 4.21	Contour plot turbulent kinetic energy 3 blades rotor hub assembly	67
Figure 4.22	Turbulent kinetic energy fuselage component for 3 blades static analysis	68
Figure 4.23	Contour plot turbulent intensity 3 blades rotor hub assembly	69
Figure 4.24	Turbulent intensity fuselage component for 3 blades static analysis	70
Figure 4.25	Contour plot dynamic pressure 4 blades rotor hub assembly	71
Figure 4.26	Dynamic pressure of fuselage component for 4 blades static analysis	72
Figure 4.27	Contour plot total pressure 4 blades rotor hub assembly	74
Figure 4.28	Total pressure of fuselage component for 4 blades static analysis	74
Figure 4.29	Contour plot turbulent kinetic energy for 4 blades static analysis.	75

Figure 4.30	Turbulent kinetic energy of fuselage for 4 blades static analysis.	76
Figure 4.31	Contour plot turbulent intensity for 4 blades static analysis.	77
Figure 4.32	Turbulent intensity of fuselage for 4 blades static analysis.	78
Figure 4.33	Facet maximum turbulent kinetic energy for 2, 3 and 4 blades elliptical fairing static analysis	79
Figure 4.34	Facet maximum turbulent intensity for 2, 3 and 4 blades elliptical fairing static analysis	80
Figure 4.35	Drag force for 2, 3 and 4 blades elliptical fairing static analysis	81
Figure 4.36	Turbulent kinetic energy and turbulent intensity elliptical static analysis point 1 and 2 of fuselage.	82
Figure 4.37	Dynamic pressure and total pressure elliptical static analysis point 1 and 2 of fuselage	83
Figure 4.38	Contour plot of dynamic pressure 2 blades rectangular static analysis	85
Figure 4.39	Contour plot of dynamic pressure 3 blades rectangular fairing static analysis.	85
Figure 4.40	Contour plot dynamic pressure 4 blades rectangular fairing static analysis	86
Figure 4.41	Contour plot total pressure for 2 blades rectangular fairing static analysis	90
Figure 4.42	Contour plot total pressure for 3 blades rectangular fairing static analysis	91
Figure 4.43	Contour plot total pressure for 4 blades rectangular fairing static analysis.	92
Figure 4.44	Contour plot turbulent kinetic energy for 2 blades rectangular fairing static analysis	94
Figure 4.45	Contour plot turbulent kinetic energy for 3 blades rectangular fairing static analysis	94
Figure 4.46	Contour plot turbulent kinetic energy for 4 blades rectangular fairing analysis	95
Figure 4.47	Contour plot turbulent intensity for 2 blades rectangular fairing static analysis	98
Figure 4.48	Contour plot turbulent intensity for 3 blades rectangular fairing static analysis	99
Figure 4.49	Contour plot turbulent intensity for 4 blades rectangular	

	fairing static analysis	99
Figure 4.50	Facet maximum turbulent kinetic energy and turbulent intensity for 2,3 and 4 blades rectangular fairing static analysis	103
Figure 4.51	Drag force for 2, 3 and 4 blades rectangular fairing static analysis	105
Figure 4.52	Dynamic pressure and total pressure rectangular static analysis point 1 and 2	106
Figure 4.53	Turbulent kinetic energy and turbulent intensity rectangular static analysis point 1 and 2	107
Figure 4.54	Main rotor hub assembly.	108
Figure 4.55	Actual model helicopter.	109
Figure 4.56	Contour plot dynamic pressure for real rotor hub static analysis	110
Figure 4.57	Close up view of dynamic pressure for $\alpha = -15^\circ$	110
Figure 4.58	Contour plot total pressure for real rotor hub static analysis	111
Figure 4.59	Close up view of total pressure for $\alpha = -15^\circ$	112
Figure 4.60	Fuselage component	113
Figure 4.61	Contour plot turbulent kinetic energy for real rotor hub static analysis	114
Figure 4.62	Close up view of turbulent kinetic energy for $\alpha = -15^\circ$	114
Figure 4.63	Contour plot turbulent intensity for real rotor hub static analysis	116
Figure 4.64	Close up view of turbulent intensity for $\alpha = -15^\circ$	116
Figure 4.65	Turbulent kinetic energy and turbulent intensity for fuselage of 2 blades rotor configurations.	119
Figure 4.66	Drag force for fuselage and rotor of 2 blades rotor configurations	120
Figure 4.67	Turbulent kinetic energy 2 blades elliptical fairing dynamic analysis	122
Figure 4.68	Turbulent kinetic energy 3 blades elliptical fairing dynamic analysis	122
Figure 4.69	Turbulent kinetic energy 4 blades elliptical fairing dynamic analysis	123
Figure 4.70	Turbulent kinetic energy cloud formed for 0.01s seconds and 0.014 seconds.	124

Figure 4.71	Cloud formed for 0.02s seconds and 0.021 seconds frames.	125
Figure 4.72	PSD Turbulent kinetic energy 2 blades elliptical fairing	127
Figure 4.73	PSD Turbulent kinetic energy 3 blades elliptical fairing	127
Figure 4.74	PSD Turbulent kinetic energy 4 blades elliptical fairing	128
Figure 4.75	Contour plot turbulent intensity 2 blades elliptical fairing	129
Figure 4.76	Contour plot turbulent intensity 3 blades elliptical fairing	129
Figure 4.77	Contour plot turbulent intensity 4 blades elliptical fairing	130
Figure 4.78	PSD Turbulent intensity 2 blades elliptical fairing dynamic analysis	131
Figure 4.79	PSD turbulent intensity 3 blades elliptical fairing dynamic analysis	131
Figure 4.80	PSD Turbulent intensity 4 blades elliptical fairing dynamic analysis	132
Figure 4.81	Summary of RMS and PSD of turbulent kinetic energy against numberof blades and frequency domain	133
Figure 4.82	Summary of RMS facet maximum and PSD of turbulent intensity against number of blades and frequency domain	134
Figure 4.83	Contour plot turbulent kinetic energy 2 blades rectangular fairing	135
Figure 4.84	Contour plot turbulent kinetic energy 3 blades rectangular fairing	136
Figure 4.85	Contour plot turbulent kinetic energy 4 blades rectangular fairing	136
Figure 4.86	PSD turbulent kinetic energy 3 blades rectangular fairing dynamic analysis	137
Figure 4.87	PSD Turbulent kinetic energy 4 blades rectangular fairing dynamic analysis	138
Figure 4.88	Contour plot of turbulent intensity of rectangular fairing 2 blades	139
Figure 4.89	Contour plot of turbulent intensity of rectangular fairing 2 blades	139
Figure 4.90	Contour plot of turbulent intensity of rectangular fairing 2 blades	140
Figure 4.91	PSD Turbulent intensity 2 blades rectangular fairing dynamic analysis	141
Figure 4.92	PSD Turbulent intensity 3 blades rectangular fairing dynamic analysis	141

Figure 4.93	PSD turbulent intensity 4 blades rectangular fairing dynamic analysis	142
Figure 4.94	Summary of turbulent kinetic energy and PSD against number of blades and frequency domain	143
Figure 4.95	Summary of RMS turbulent intensity and PSD against number of blades and frequency domain	144
Figure 4.96	PSD turbulent kinetic energy data between elliptical and rectangular fairing dynamic analysis.	145
Figure 4.97	Contour plot turbulent kinetic energy of 1600 rpm dynamic analysis	146
Figure 4.98	PSD Turbulent kinetic energy 1600 rpm dynamic analysis	147
Figure 4.99	Contour plot turbulent intensity 1600 rpm dynamic analysis	148
Figure 4.100	PSD turbulent intensity 1600 rpm dynamic analysis	149
Figure 4.101	Contour plot turbulent kinetic energy 1400 rpm dynamic analysis	150
Figure 4.102	PSD Turbulent kinetic energy 1400 rpm dynamic analysis	151
Figure 4.103	Contour plot turbulent intensity for 1400 rpm dynamic analysis	152
Figure 4.104	PSD turbulent intensity 1400 rpm dynamic analysis	152
Figure 4.105	Contour plot for dynamic pressure 1200 rpm dynamic analysis	154
Figure 4.106	PSD dynamic pressure 1200 rpm dynamic analysis	154
Figure 4.107	Contour plot total pressure for 1200 rpm dynamic analysis.	155
Figure 4.108	PSD total pressure 1200 rpm dynamic analysis	156
Figure 4.109	Contour plot of turbulent kinetic energy for 1200 rpm.	156
Figure 4.110	PSD turbulent kinetic energy 1200 rpm dynamic analysis	157
Figure 4.111	Contour plot of turbulent intensity of 1200 rpm dynamic analysis	158
Figure 4.112	PSD Turbulent intensity 1200 rpm dynamic analysis	158
Figure 4.113	Simplified model without fairing	159
Figure 4.114	Turbulent Kinetic Energy for $\alpha = -5^\circ$	160
Figure 4.115	Turbulent kinetic energy comparison for 1200 rpm, 1400 rpm and 1600 rpm.	160
Figure 4.116	TKE and TI of 2 blades elliptical and actual rotor for 1200	

rpm

162

Figure 4.117 Turbulent kinetic energy and turbulent intensity for 2 blades rotor of dynamic analysis for 1200 rpm.

163

CHAPTER 1

INTRODUCTION

1.1 Background

Helicopter is a wingless aircraft that can attain vertical flight from the gyration of overhead blades (Brain et al., 2018). Helicopter runs through revolution of blades that forming a lift (Robert, 2017). Its ability to fly in multiple directions has been admired vigorously. Flight condition and duration are crucial as thehelicopter itself (Lombardo, 1993). De Jonge (1986), stated that helicopter manoeuvre results in a number of continuous incremental load of cycles as compared to a fixed wing. Advance helicopter design continuously focuses on implementation of a better and faster helicopter. However, the intricate geometry or rotational effect does play a vital role in the production of hub drag (Raghav et al., 2013). Large eddy motion usually found in the formation of an unsteady wake, which shed downstream along the tail boom of the helicopter, usually create irregular frequency. As the unsteady wake hits the vertical tail rotor, the impact causes the formation of tail shakephenomenon. The aerodynamic interaction between a rotor and fuselage is complex and difficult problems. Understanding the component on the helicopter plays an important role in knowing the parts that involved in initiation of unsteady wake. Engine, main rotor and tail rotor are important key parts in flight formation; however, each component contributes to its own mechanical vibration. Therefore, investigation on the presence of unsteady wake will be the focus especially the unsteady wake interaction on main rotor hub assembly.

1.2 Importance of Rotor System

Helicopter is known for its specialty and uniqueness through their ability to manoeuvres in multiple directions during flight (Lombardo, 1993). However, everything comes with limitation. To obtain a better flight quality for a helicopter, new technology and ideas had been presented. Even though many aeronautic companies had come with various designs of helicopter with certain functionality, yet, it all comes down to blades of the rotor. Rex (2020) stated that vibrations and vibratory loads propagated through the rotor system into fuselage through rotor shaft and flexible control linkage, mechanically. Similarly, as stated by Wang (2020), to improve a helicopter ride, designers were required to minimise the vibration, which mostly originates from the rotor and interface with fuselage. De Jonge (1986) stated that it was difficult to accurately predict the rotor blade loading since it has to currently follow up with air worthiness requirements and fatigue analysis must be based on the existing measured loads. David (1986) and Brocklehurst (2013) had done a research on the characteristic of the optimum dynamic and a review paper on various design of rotor blade tip, which determined the best design and highest lift recorded. A desirable flight condition such as producing the best lift with minimum drag and fuel consumption is favourable. This project, concentrating on the main rotor hub assembly itself. There were few scholars who did a design on the main rotor hub to reduce the drag produced, for example, by Khier (2012). Khier (2012) stated that one third of the total drag on a modern conventional helicopter is attributed to the rotor hub and major contributor to the tail shake phenomenon (Cassier, 1994). Tail shake phenomenon relates to an anti-torque system, especially during forward flight, whereby, in this state, the highly unsteady main rotor wake strikes onto the tail boom and empennage, which excites a fluctuation of the lateral bending moment on the helicopter fuselage (Kowarsch et al., 2014). This high vibration level is considered to be unfavourable. Figure 1 shows the anti-torque system of the helicopter that is used to counter the torque production from the blade rotation.



Figure 1 Anti-torque rotor produces thrust to oppose torque (FAA ,2012).

Anti-torque system or also known as tail rotor is one of the control system that was design to help counter the torque created from the blade rotation. Through the control panel, the flight crew vary the thrust located on the tail rotor to maintain the direction of flight, especially during yaw or changing heading while hovering(Federal Aviation Administration, 2012). Tail rotor acts as the mounting for a single tail rotor as it creates torque during helicopter turns, whereas the rotor blades generate yawing effect (Padfield,1996). It is stated that in achieving a static stability even in the directional mode, the yawing derivative, Cn_{β} must be a positive value whereby it will turn to its balance condition when subjected to a yawing disturbance (Nelson,1998). However, the focus of this project is to investigate the formation of an aerodynamic unsteady wake on main rotor hub which leads to the creation of tail shake phenomenon. There are two parts of the system that play crucial roles in flight and stability in unsteady wake investigation which are the main rotor and tail rotor.

1.3 Interaction of Unsteady Wake

Turbulent formation usually occurs due to disturbance of air flow surround or through an area that divert the original flow. Reduction or an increment of velocity due to surface roughness effects the generation of turbulent. It can be visibly seen on wingtip of a fixed wing during high speed flight whereby vortices occur due to the pressure differential over the wing surfaces (IVAO, 2018). Jimenez et al. (2016) stated that fuselage is one of the main contribution of a parasite drag which supported

by Raghav et al. (2013) whereby 50% to 70% of drag generated by the fuselage of a helicopter that included both the main rotor fairing and hub. The complex geometry of the main rotor hub is one of the reason for the generation of unsteady wake that been said to contribute 25% to 30% of aircraft parasite drag (Kowarsch, 2014). Kowarsch (2014) listed that without the main rotor hub cap, it reduces the parasite drag portion by 5.7%, however, in the design stage of a helicopter, the number of rotor blade is crucial since it is closely related to main rotor hub assembly. The number of blades relatively dependent in the mission and weight of the aircraft. Most helicopter with one or two passengers tends to be assembled with a single rotor blade. Robinson R22 is one of lightweight helicopter that commonly employed for surveying purposes whereby it is assembled with a single rotor blade. However, helicopter such as Chinook CH-47 is design for military mission and for heavy lifting, therefore the ideal CH-47 assembled with six rotor blades. The angle difference on rotor blades could cause the existenceof a wake turbulence. Moreover, the interference between the geometry of fairings and number of blades could lead to an increase of turbulent wake formed on the aft of a helicopter. In this paper, different number of blades and design of fairings will be used to observe the interference effects of geometry and number of blades in the formation of turbulent. Also, to prove either in the presence of hub cap or fairings, the wake frequency will be reduced. Figure 1.1 shows the area that believed to be contributing to the production of unsteady wake and tail shake phenomenon.



Figure 1.1 Main rotor hub assembly (FAA, 2012).

During the forward flight, the geometry on the main-rotor-hub assembly includes the number of main-rotor blades believed to contribute to the formation of unsteady wake. Physically, the geometries of the main-rotor-hub assembly can be seen to have sharp edges and irregular surfaces that deflects the free stream flow. Refer the blades rotation into an element, which is labelled in red and black, as shown in Figure 1.2. Velocity is the best parameter used to explain and visually show the derivatives or changes that occurred during the flight. Figure 1.2 shows the adverse velocity generated along the main rotor blade. The analysis is based on the location of the element that moves further away from the hub with the velocity produced, also known as tip speed. During a normal rotation of blades, the red label element has higher velocity as compared to an element in black label whereby it is position closer to the centre of the main rotor hub.

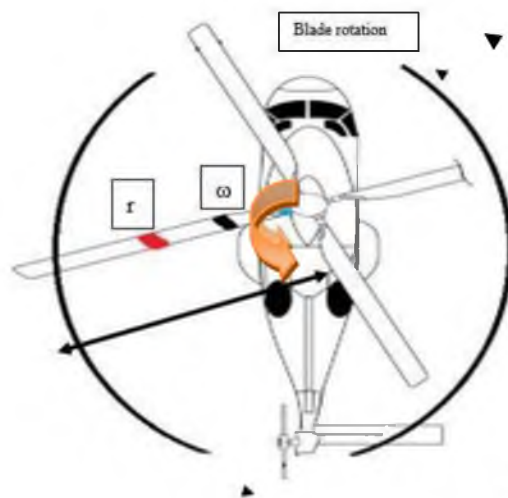


Figure 1.2 Velocity differences along the main rotor blades

Equation (1) shows the relationship between the velocity of a blade element and the distance of an element to the centre of the hub.

$$V = \omega r \quad (1)$$

Where; the V = blade velocity, (m/s)

ω = angular velocity (revolution per min)

r = distance from the centre of hub to the colour label, (m)

Equation (1) shows that the velocity is proportional to the distance from centre of the hub, r . It is proven that velocity increase as the well as the blade length increases. The speed of the tip of the blades is greater related to the speed of the blades which closer to the main rotor hub. The velocity difference causes the formation of velocity in irregular magnitude along the main-rotor blades. This produces pressure differential, which at particular pitch angle may cause the tail shake phenomenon. Figure 1.3 shows the top view of a helicopter that is assumed to be in a control system, with incompressible flow at forward flight condition. The velocity derivatives at the tip of the blades would produce higher velocity with an additional of free stream flow velocity. Stream flow increases the level of velocity as it is further way from the centre of rotation. The irregular velocities along the main-rotor blade generated are one of the causes of the uneven wake of the main rotor hub.

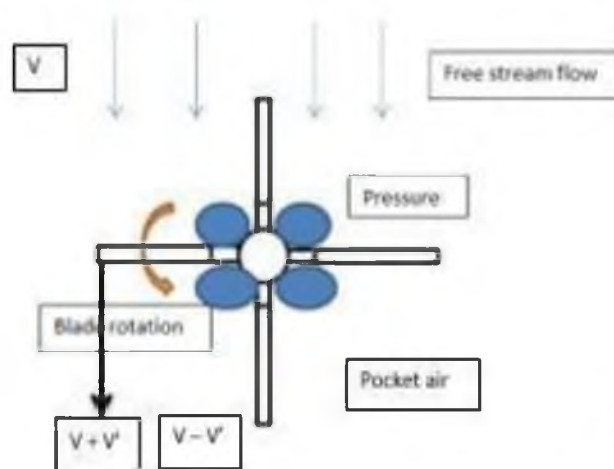


Figure 1.3 Velocity difference between the tip and the centre of the rotation.

Where,

V = Free stream flow velocity

V' = Derivative of velocity.

The adverse velocity along the rotor blades causes an adverse pressure, which leads to the formation of turbulent and wake. The cyclic load of blades generates an alternate form of adverse pressure in the form of air pocket. During forward flight, these air pocket's adverse pressure travel towards the aft post of fuselage and hit the

tail rotor continuously, whereby it leads to a so-called tail shake phenomenon. Vibration typically occurs between one and two times the rotor rotational frequency (Waard & Trouve, 1999). The wake of the main rotor, the rotor hub and the airframe that imposes on the tail boom, causing an excitation of low-frequency of the entire helicopter airframe (Schaeferlein et al., 2017). Figure 1.4 shows the visual formation of unsteady wake sourced out from main rotor assembly.

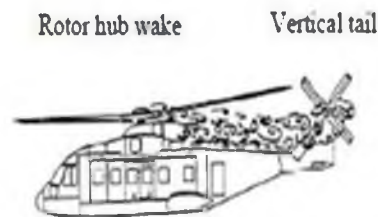


Figure 1.4 Schematic of tail shake phenomenon (Waard and Trouvé, 1999)

The unsteady wake was justified to affect the control performance and safety of the helicopter structure. It is said to be complicated and leads to a complexity in understanding the aerodynamics itself (Hassan et al., 1999). Supported by Roesch and Dequin (1983) who stated that tail shake helicopter phenomenon caused the disturbance in performance, passenger's comfort and control quality. Interactional Aerodynamics (I/A) still remain a prolonged issue for continuous investigation. This is also agreed by Schaeferlein (2017), whereby such phenomenon described a significant interaction of the rotor wake with structure of the airframe leading to the flight instability and reduction in ride comfort.

A wind tunnel is an unwieldy device that needs continuous monitoring and maintenance as compared to Computational Fluid Dynamic (CFD) which is a modern instrument that helps to reduce the time and cost of a simulation. However, a validation stage through grid independent study is required. It is to comprehend the capabilities of the software and the computer itself. Without validation, it cannot be a definite result. Vertical tail and the main rotor hub interaction is said to be the consequence of tail shake phenomenon, although the researcher's hard work and a lot of effort given, yet little information of tail shake phenomenon had been made (Coton, 2009). Coton

(2009) said it was due to most data which were kept sensitive and private from most researchers.

1.4 Problem statement

The rotor hub system is one of the primary contributors to the helicopter parasite drag and inherent limiters to maximise the helicopter forward-flight speed (Reich et Al., 2016). Previous conducted study stated that one third of the total drag was generated from the rotor hub and this statement achieved from the analysis conducted on a modern conventional helicopter (Khier, 2012). Supported by Schaeferlein (2017), that rotor hub fairing, engine exhaust, cowling, the shape, position and dynamics of the tail boom play a key role in the characteristics of the tail shake phenomenon. Minimalising the production of drag is very much desired and an essential step in developing an operative, effective helicopters. However, the main rotor hub assembly believed to be the foremost contributor in tail shake phenomenon (Cassier, 1994). Interactional Aerodynamics (A/I) is complex even after experiencing and conducting many works, yet it is still hard to confidently predict the result without any flight test of a new design helicopter (Waard & Trouvé, 1999). Due to sensitivity issues, most helicopter manufacturer tended to keep the A/I data away from most researchers and reduces the chances of understanding the complexity of tail shake phenomenon.

Variation of time makes unsteady flow to be difficult and complicated as compared to a steady flow (Brock et al., 1972). In maintenance of an aircraft, some parts are required to undergo periodic maintenance based on the system cyclic. Through a continuous hours of flying, vibration is not something yet to be avoided by any mechanical system. Through unsteady wake formation source from the main rotor hub, it will create a tremor on the helicopter's tail boom that generates continuous vibration which leads to poor control performance and responsive quality of the helicopter. Excessive vibration and additional of external forces reported to be one of the reason of any helicopter crashed incident. Wake is divided into near and far wake which comprised trailed and shed vorticity which later on created vortex (Xu Guo et

Al., 2002). The pulsation frequency plays the main part in the helicopter crash incident. The low induced velocity of the main rotor as well as the additional descent rate leads to a strong interaction between the main rotor wake and tail boom (Schaeferlein et al., 2017). A subtle frequency existed as the rotor blades rotation been disrupted, however, with presence of outward forces, an intermediate vibration could be generated leading to disengagement of loose components on helicopter. A high frequency vibration can be detected especially when the tail rotor, tail drive cable and shaft, tail fan shaft vibrates equally or beyond the speed of tail rotor. In any circumstance, whereby the main rotor hub assembly wake coincides with the natural frequency on the tail section, a robust intensification would occur which leads to an impulsive structural failure that may transpire due to fatigue problems. Addition of drag can be detected from the tail shake phenomenon that leads to poor handling and comfort. Moreover, the stability characteristic such as yawing and pitching can be affected (Ishak, 2012). By using the Computational Fluid Dynamics (CFD), an investigation on unsteady flow of air at constant velocity, various rotational speeds, and in different pitch angle, would help in understanding the effects of the unsteady wake produced from the main rotor hub assembly. It is important to perceive the outcome of the unstable flow under selected flight parameters. study Previous study researcher on the low range advance ratios of up to 0.3. However, the air load pressure is believed to be quite small for both the low and high pitching positions indicating that the wake generated is too small to influence the flow surrounds in the vicinity of tail parts (Leishman et al., 1996). Obviously, higher advance ratio works are highly demanded and this paper focuses on investigating the effects of high advance ratio towards the wake formation.

1.5 Objectives

- 1) To investigate the unsteady aerodynamic load characteristics triggered by the unsteady wake of the helicopter's main rotor-hub assembly through numerical simulation.
- 2) To evaluate the static and dynamic analyses of unsteady wake of main rotor-hub assembly of a simplified and real rotor models for different flight configurations.

1.6 Scopes of Study

The following are the scopes that will be covered:

1. Develop a simplified three-dimensional model of the main-rotor-hub helicopter for unsteady wake analysis.
2. Simulations on the actual helicopter model by using CFD software with various helicopter configurations and flight parameters.
3. Flight parameters and configurations that shall be studied:
 - i) Advance ratio / rotational speed
 - ii) Number of main rotor blades
 - iii) Configurations
 - iv) Angle of attack (α)
4. CFD results will be validated with experimental results conducted by other researchers.

From the selected flight configurations, this paper will be able to observe the formation of adverse pressure gradient surrounding the simplified and real rotor model. Quantified the amount of turbulent, pressure and drag generated and compared the effects of stream flow due to complex geometry and employment of fairing on the after wake for static and dynamic analyses.

REFERENCES

- Ahmed, T., Amin, M. T., Islam, S. M. R., & Ahmed, S. (2013). Computational Study of Flow Around a NACA 0012 Wing Flapped at Different Flap Angles with Varying Mach Numbers. *Global Journal of Researches in Engineering*, 13 (4), 1–13.
- Auiler, J.E., 1971. Use of the turbulence kinetic energy equation in analysing turbulent near wakes.
- Autodesk (2014) *Computational Fluid Dynamic Support and Learning*. [Online] Available from: [Autodesk | 3D Design, Engineering & Construction Software](#). [Accessed: 30 December 2019]
- Bakker, A., 2002. Lecture 9-kolmogorov's theory applied computational fluid dynamics. *Educational material*. © *Fluent Inc*.
- Batrakov, A., Garipova, L., Kusyumov, A., Mikhailov, S., & Barakos, G. (2015). Computational Fluid Dynamics Modeling of Helicopter Fuselage Drag. *Journal of Aircraft*, 52(5), 1634–1643. <https://doi.org/10.2514/1.C033019>
- Brand, A.G., McMahon, H.M. and Komerath, N.M., 1990. Correlations of rotor wake/airframe interaction measurements with flow visualization data. *Journal of the American Helicopter Society*, 35(4), pp.4-15.
- Brain, Marshall & Harris (2018), [Online] Available from: <https://science.howstuffworks.com/transport/flight/modern/helicopter1.html>. [Accessed: 20 February 2019]
- Brain M, Harris W., n.d, *Flying a Helicopter: Directional Flight*, [Online] Available from: [Flying a Helicopter: Directional Flight - How Helicopters Work | HowStuffWorks](#). [Accessed: 27 April 2021]
- Brocklehurst, A., & Barakos, G. N. (2013). A review of helicopter rotor blade tip shapes. *Progress in Aerospace Sciences*, 56, 35–74.
- Brock, A. E. and Houghton, E. L. (1972). *Aerodynamics for an engineering student*, London, Butler & Tanner Ltd., Frome.
- Cassier, A.Weneckers, R. and Pouradier J.M., (1994). Aerodynamic development of the Tiger helicopter. *50th American Helicopter Society Forum*, May 1994.

- Cooke W. G. (2003), *UH-60A Black Hawk*, [Online] Available from: [UH-60A BLACK HAWK \(SIKORSKY\) \(inetres.com\)](http://UH-60A.BLACK HAWK (SIKORSKY) (inetres.com)). [Accessed: 27 April 2021].
- Costes, M, Beaumier P., Bettschart N., Servera G., (2000). *Computational Tools Used at ONERA for the Description of Helicopter Rotor Wakes*. AIAA 2000-0113.
- Coton, F., (2009), "Evaluation of UTM Research Projects." Professor of Low-Speed Aerodynamics, Department of Aerospace Engineering, University of Glasgow.
- Cosner R.R., Rahaim C.P. (2001). The AIAA Committee on Standards for CFD. Retrieved on February 19,2018, from www.qnet-cfd.net/workshop/1st/pdf/02_in1_aiaa.pdf
- David P. A., Rossow, M. P., Korn, A., & Ko, T. (1986). Design of helicopter rotor blades for optimum dynamic characteristics. *Computers and Mathematics with Applications*, 12(1 PART A), 85–109
- Davidson, L., 2015. An introduction to turbulence models.
- De Jonge J.B, (1986), *Loads and Damage Tolerance for Helicopters*, National Aerospace Laboratory NLR, NLR TR 86018L.
- De Gregorio, F., (2012). Flow field characterization and interactional aerodynamics analysis of a complete helicopter. *Aerospace Science and Technology*, 19(1), 19–36.
- Eleni, Douvi C., Tsavalos I. Athanasios, and Marmaris P. Dionissios, (2012)"Evaluation of the turbulence models for the simulation of the flow over a National Advisory Committee for Aeronautics (NACA) 0012 aerofoil." *Journal of Mechanical Engineering Research* 4.3: 100-111.
- Efluids (2021) *Bernoulli's equation*. [Online]. June 2021. Available from: [Bernoulli's Equation \(princeton.edu\)](http://Bernoulli's Equation (princeton.edu)). [Accessed from: 15 June 2021].
- Federal Aviation Administration. (2012). Helicopter Components, Sections, and Systems. *Helicopter Instructor's Handbook*, 183.
- Hall, N. (2021) *Shape Effects on Drag*. [Online]. Available from: [Shape Effects on Drag \(nasa.gov\)](http://Shape Effects on Drag (nasa.gov)) [Accessed: 4 December 2020].
- Hassan, A., Thompson, T., Duque N., Melton, J. (1999). Resolution of tail buffet phenomena for AH-64DTM Longbow ApacheTM. *Journal American Helicopter Society*, Volume 44.
- Helgesson, M., 2015. Response of a rocket nozzle to power spectral density loads.
- Ishak, I.S., 2012. *Unsteady Aerodynamic Wake Of Helicopter Main-Rotor-Hub Assembly* (Doctoral dissertation, Universiti Teknologi Malaysia).
- IVAO, International Virtual Aviation Organization, (2018), *Wake Turbulence*.
- Jimenez A. G., Barakos G., (2016). CFD Analysis of Hover Performance of Rotors at

Model-Scale Condition. *The Aeronautical Journal*, Vol. 120, Issue (1231), pp(1386-1424).

- Kenyon, A.R. and Brown R.E. (2007). Wake Dynamics and Rotor – Fuselage
- Khier, W. (2012). Numerical Analysis of Hub and Fuselage Interference to Reduce Helicopter Drag.
- Khier, W., 2014. Computational investigation of advanced hub fairing configurations to reduce helicopter drag.
- Kumar, S.M., 2008. Analyzing random vibration fatigue. *ANSYS Advantage*, 2(3), pp.39-42.
- Koushik, S. N. (2007). A new experimental approach to study helicopter BVI noise.
- Leishman, J.G. and Moedersheim, E., 1996. Aerodynamic interactions between a helicopter rotor and a T-tail empennage.
- Lombardo, D. C. (1993). Helicopter Structures - A Review of Loads, Fatigue Design Techniques and Usage Monitoring, (ARL-TR-15).
- Lorber P., & Egolf T., (1988), An Unsteady Helicopter Rotor-Fuselage Interaction Analysis. *NASA Contractor Report 4178*. September 1988.
- Luce, H., Kantha, L., Hashiguchi, H., Lawrence, D. and Doddi, A., 2018. Turbulence kinetic energy dissipation rates estimated from concurrent UAV and MU radar measurements. *Earth, Planets and Space*, 70(1), pp.1-19.
- Martinez I. (1996). *Termodinamica Basica Aplicada*. [Online]. Madrid, Spain: Dossat. Available from: [Termodinamica basica y aplicada1.pdf \(upm.es\)](http://www.upm.es/~termodinamica/basica_y_aplicada1.pdf). [Accessed: 27 April 2021]
- Moedersheim E., & Leishman G., (1998), Investigation of Aerodynamic Interactions Between a Rotor and a T-Tail Empennage. *American Helicopter Society*. Vol.43, Issue (1), pg(37-46).
- NASA, (2018), *2D NACA 0012 Airfoil Validation Cases*, [Online] Available from: http://turbmodels.larc.nasa.gov/naca0012_val.html. [Accessed: 14 December 2017]
- Nelson R.C., (1998). *Flight Stability and Automatic Control*. (2nd Ed.). McGraw-Hill.
- Ortega, F.T. (2011). Deconstructing Hub Drag. American Institute of Aeronautics and Astronautics
- O'Neill, C. R. (2000). Determination of Flight Stability Coefficients Using a Finite Element Cfd A B. *Design Build*, 1–16.
- Padfield G. D., (1996). Helicopter Flight Dynamics: The Theory and Application of Flying Qualities and Simulation Modelling. Blackwell Science.

- Prakash J., (2019), *Top 10 Reasons for Computer Freezing*. [Online] Available from: [Top 10 Reasons for Computer Freezing: PC Hang UP \(stellarinfo.com\)](https://stellarinfo.com/top-10-reasons-for-computer-freezing-pc-hang-up/). [Accessed: 22 March 2020].
- Pitsch, H. (2014) *Turbulence*. [Online]. Available from: [PowerPoint-Präsentation \(princeton.edu\)](https://www.princeton.edu/~hjp1/papers/Turbulence.pdf) . [Accessed: 15 December 2020]
- Raghav, V., Shenoy, R., Smith, M., & Komerath, N. (2013). Investigation of drag and wake turbulence of a rotor hub. *Aerospace Science and Technology*, 28(1), 164–175.
- Reich, D., Shenoy, R., Smith, M. and Schmitz, S., 2016. A review of 60 years of rotor hub drag and wake physics: 1954–2014. *Journal of the American Helicopter Society*, 61(2), pp.1-17.
- Reich, D., Willits, S. and Schmitz, S., 2017. Scaling and configuration effects on helicopter rotor hub interactional aerodynamics. *Journal of Aircraft*, 54(5), pp.1692-1704.
- Rex, W., Rinker, M. and Hajek, M., 2020. Sensitivity Study of Helicopter Vibrations and Loads with Elastic Fuselage Coupling and Empennage Loads from Free Wake Analysis. In *Vertical Flight Society's 76th Annual Forum and Technology Display 2020*.
- Robert, Calia (2017), *What are three types of helicopter vibration*, [Online] Available from: <https://careertrend.com/info-8547935-3-types-helicopter-vibrations.html>. [Accessed: 14 December 2017]
- Roesch P. and Dequin A., (1983), Experimental Research on Helicopter Fuselage and Rotor Hub Wake Turbulence, *Journal of the American Helicopter Society*, Volume 30, Number 1, 1 January 1985, pp. 43-51(9)
- Schaferlein U., Kessler M., Kramer E., (2017). Aeroelastic Simulation of the Tail Shake Phenomenon. *European Rotorcraft Forum*, September 2017.
- Sentker, A. and Riess, W., 2000. Experimental investigation of turbulent wake–blade interaction in axial compressors. *International Journal of Heat and Fluid Flow*, 21(3), pp.285-290.
- Stalewski, W. and Żóltak, J., 2012, September. Optimisation of the helicopter fuselage with simulation of main and tail rotor influence. In *Proceedings of the 28th ICAS Congress of the International Council of the Aeronautical Sciences, ICAS, Brisbane, Australia* (pp. 23-28).
- Simscale (2021) *K-Omega and K-Omega SST*. [Online]. May 2021. Available from: <https://www.simscale.com/docs/simulation-setup/global-settings/k-omega-sst/>. [Accessed: 10th May 2021]
- Stephen K. G., & Layton, D. M. (1983). Guide for Conceptual Helicopter Design.

- Stepanov R., Zherekhov V., Pakhov V., Mikhailov S., Garipov A., Yakubov W., and Barakos N. G., Experimental Study of Helicopter Fuselage Drag. *Journal of Aircraft*, Vol. 53, No. 5(2016), pp. 1343-1360
- Sheridan, P.F., and Smith, R.P. (1980). Interactional Aerodynamics – A New Challenge to Helicopter Technology. *Journal of the American Helicopter Society*, Vol. 25, No. 1
- Stull, R.B., 1988. Turbulence kinetic energy, stability and scaling. In *An introduction to boundary layer meteorology* (pp. 151-195). Springer, Dordrecht.
- Visaya (2016) *Static pressure vs total pressure vs dynamic pressure*. [Online]. Available from: [Static pressure vs total pressure vs dynamic pressure | Visaya](#). [Accessed: 20 March 2021].
- Waard de P.G. and Trouve M., (1999), Tail Shake Vibration: Objective Comparison of Aerodynamic Configurations in a Subjective Environment, National Aerospace Laboratory, NLR, pp -25.
- Wang, S., Han, J., Yun, H. and Chen, X., 2020. CFD-CSD method for coupled rotor-fuselage vibration analysis with free wake-panel coupled model. *Proceedings of the Institution of Mechanical Engineers, Part G: Journal of Aerospace Engineering*, p.0954410020976512.
- Xu G. H., Zhao Q. J., Gao Z., Zhao J. G., Prediction of Aerodynamic Interactions of Helicopter Rotor on its Fuselage. *Chinese Journal of Aeronautics*, Vol.15, No. 1, pg 12-17.
- Yu, H., Geng Qi, W., Hai Lang, Z., Xu Yang, F. and Hussain, F., 2019. The effects of advance ratio and blade number on the forward flight characteristics of cycloidal rotor. *Proceedings of the Institution of Mechanical Engineers, Part G: Journal of Aerospace Engineering*, 233(2), pp.573-588.

LIST OF PUBLICATIONS

Conference Proceeding

- 1) Othman, N., Ishak, I.S. and Dahalan, M.N., Numerical Studies on Turbulence Modelling of Symmetrical Aerofoil. *Sharing Visions and Solutions for Better Future*, p.192.

Indexed Journal

- 1) Othman, N., Ishak, I.S. and Dahalan, M.N. (2021) ‘Static Analysis of Unsteady Aerodynamics Wake of Simplified Helicopter Model via Simulation Work’, *Journal of Advanced Research in Fluid Mechanics and Thermal Sciences*. (Accepted)